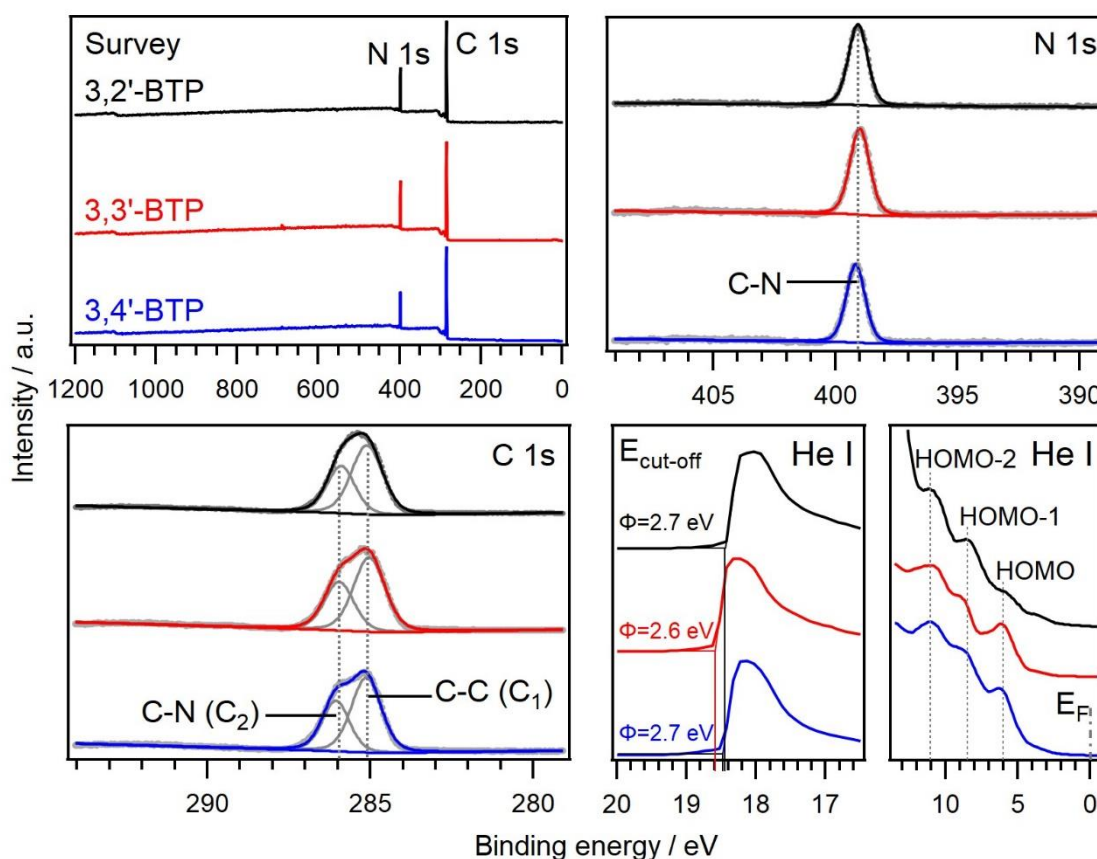


**Influence of regioisomerism in bis(terpyridine) based  
exciplexes with delayed fluorescence**  
***Supplementary Information***

*A. Lennart Schleper, Sabina Hillebrandt, Christoph Bannwarth, Andreas Mischok, Seonil Kwon, Florian Buchner, Francisco Tenopala-Carmona, R. Jürgen Behm, Felix D. Goll, Philipp J. Welscher, Michael Usselman, Ulrich Ziener,\* Malte C. Gather,\* and Alexander J. C. Kuehne\**

## Physical Characterization of the individual BTPs

Ultraviolet photoelectron spectroscopy on pure BTP films on silicon wafers were carried out in a commercial UHV system (SPECS) with a base pressure of  $2 \times 10^{-10}$  mbar. It is equipped with a non-monochromatized X-ray source (SPECS XR50, Al- $K_{\alpha}$  and Mg- $K_{\alpha}$ ), a monochromatized X-ray source (SPECS XR50M, Al- $K_{\alpha}$  and Ag- $K_{\alpha}$ , FOCUS 500 X-ray monochromator), a He lamp (SPECS UVS 300) and a hemispherical analyzer (SPECS, DLSEGD-Phoibos-Has3500) for XPS and UPS measurements. The XP spectra were recorded using monochromatized Al  $K_{\alpha}$  radiation ( $h\nu^0 = 1486.6$  eV) at a power of 400 W ( $U = 15$  kV,  $I = 26.7$  mA), with a pass energy of 20 eV for all detail spectra. Peak fitting was performed using the Igor pro 8.04 software; all peaks were fitted with a simultaneous fit of the background (Shirley + slope) and signal, assuming a pseudo-Voigt type peak shape, which is a linear combination of a Gaussian and a Lorentzian function. The binding energy (BE) scale was calibrated by setting the position of the C-C-related peak ( $C_1$ ) of the BTPs to 285.1 eV according to the BE of adsorbed benzene multilayers).<sup>1,2</sup> For the UPS measurements (He I:  $h\nu = 21.2$  eV) a bias voltage of  $-5.0$  V was applied to the sample to accelerate the photoelectrons into the analyzer (pass energy  $E_{\text{pass}} = 1$  eV). Here, the energy scale was adjusted such that the Fermi level ( $E_F$ ) is located at 0 eV BE. The position of the Fermi level was determined from the UP spectrum of a Ru(0001) crystal.



**Figure S1** | X-ray and ultraviolet photoelectron spectroscopy of the BTPs to extract ionization potentials and HOMO energies.

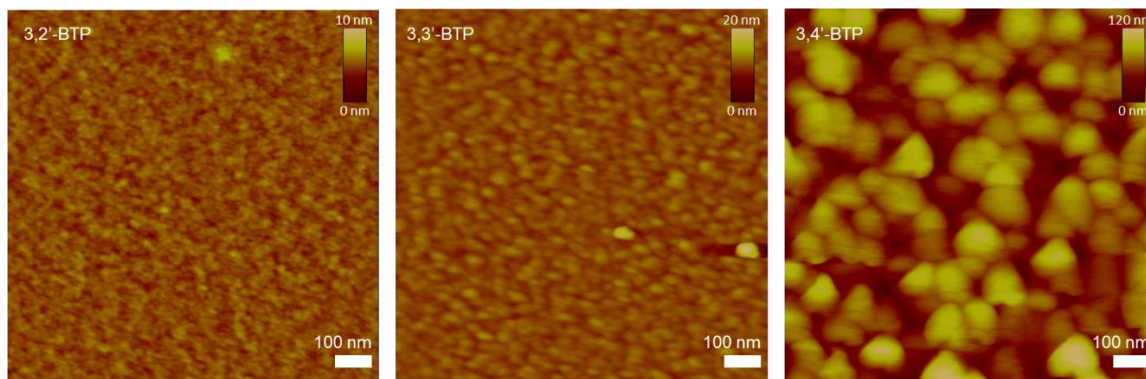


**Figure S2** | Atomic force micrograph of BTPs evaporated as 40 nm thick films onto Si-wafer. 3,2'- and 3,3'-BTP deposit as flat films, while 3,4'-BTP deposits as islands that grow into globes.

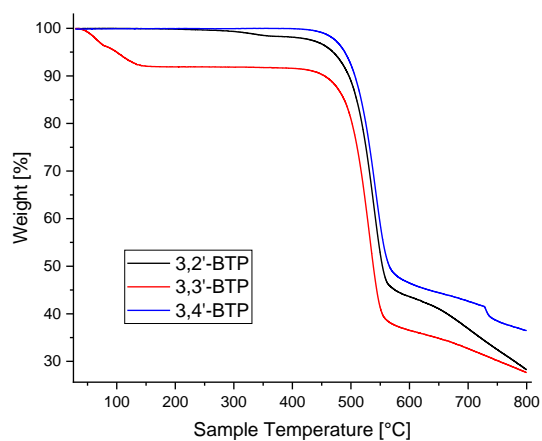


**Figure S3** | Thermogravimetric analysis (TGA) of the BTP compounds to determine their decomposition temperatures  $T_{dec}$ .

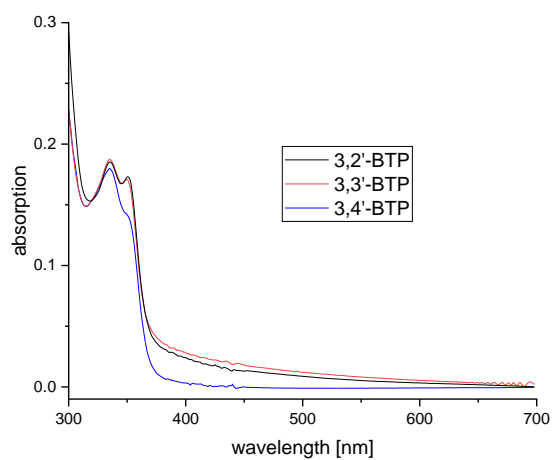


**Figure S4** | UV-vis spectra of BTPs.

## Photolumuminescence of TCTA:BTP exciplexes in thin films

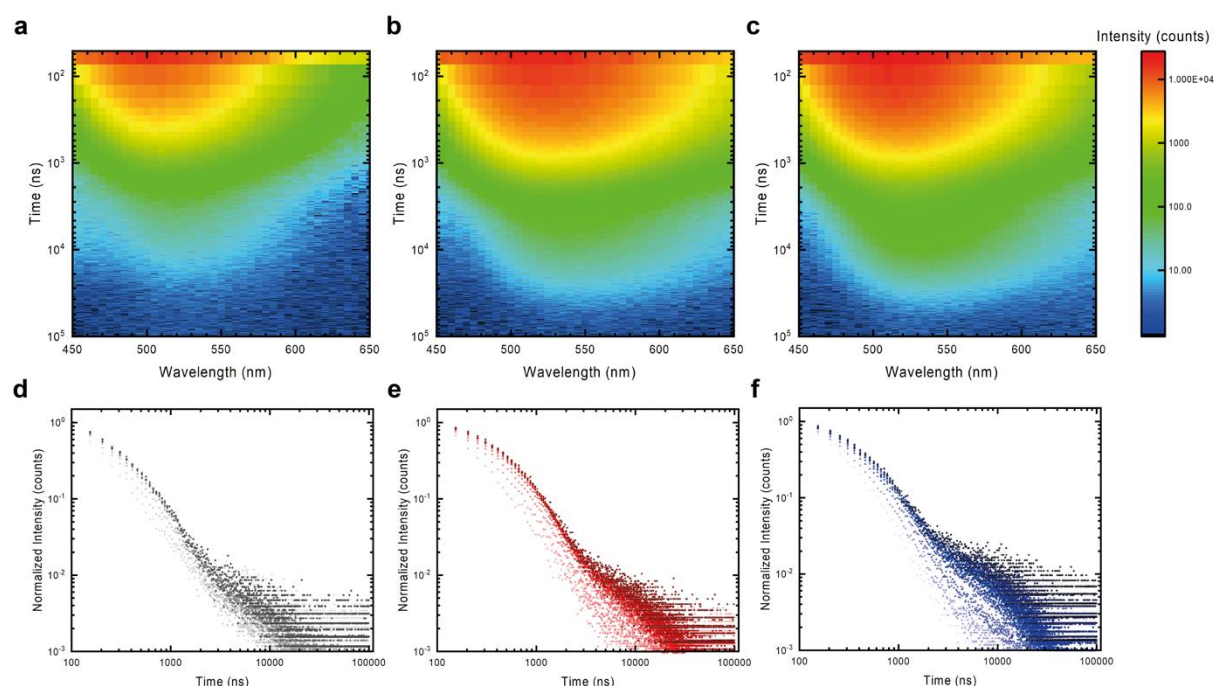


**Figure S5** | Transient photoluminescence spectra (a-c) and decay traces (d-f) at selected wavelengths between 450 and 650 nm of the TCTA:3,2'-BTP (a,d), TCTA:3,3'-BTP (b,e), and TCTA:3,4'-BTP (c,f) exciplexes. Darker colored decay traces in d-f correspond to longer emission wavelengths.

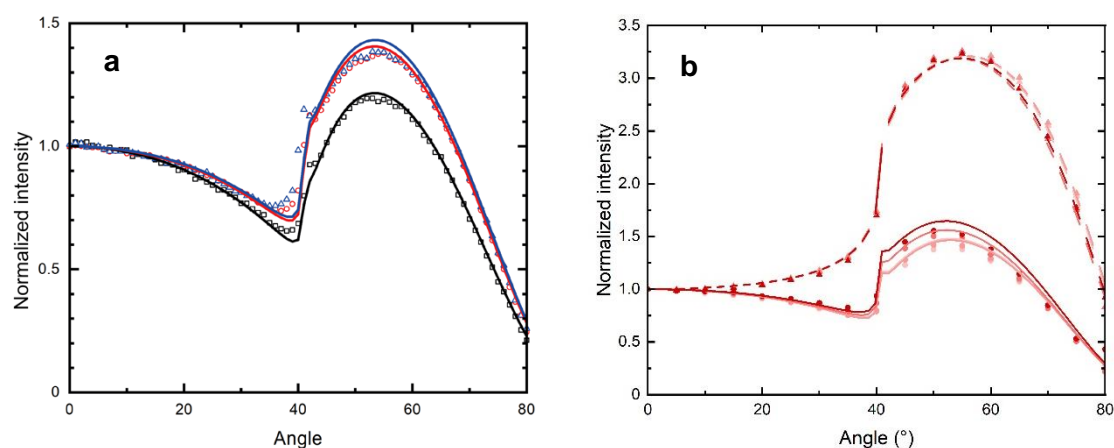


**Figure S6** | Normalized angle-resolved photoluminescence intensity for (a) TCTA:3,2'-BTP (black), TCTA:3,3'-BTP (red), and TCTA:3,4'-BTP (blue) exciplexes – p-polarized components. Simulated fits (solid line) correspond to  $a = 0.362$  (TCTA:3,2'-BTP),  $a = 0.412$  (TCTA:3,3'-BTP), and  $a = 0.385$  (TCTA:3,4'-BTP). (b) 5% ( $a = 0.398$ ), 10% ( $a = 0.400$ ), 15% ( $a = 0.420$ ), and 20% ( $a = 0.443$ ) of 3,3'-BTP in TCTA, color coded in the figure by the gradient from light red to darker (for increasing percentage of 3,3'-BTP). Triangles represent s-polarized and circles p-polarized components.

## Simulated exciplex structures

We performed a conformational analysis for the BTP systems and TCTA at the GFN2-xTB level using the frameworks implemented in the CREST and xTB programs.<sup>3-6</sup> The conformational search is based on metadynamics, molecular dynamics and genetic crossing steps (option “v3” in the CREST program). The structures within 3 kcal/mol were then reoptimized at the PBEh-3c level of theory.<sup>7</sup> This is an efficient composite density functional theory (DFT) method with corrections for dispersion interactions (via the D3 model) and basis set superposition errors.<sup>8-10</sup> It has been specifically designed to describe non-covalent interactions and geometries with good accuracy at comparably low computational cost. All density functional theory calculations were performed with the program Turbomole suite.<sup>11</sup>

We then used the intermolecular force-field xTB-IFF, which is based on the GFN1-xTB electronic structure, to dock the BTP and TCTA geometries.<sup>12,13</sup> The resulting geometries were then reoptimized with GFN2-xTB and, subsequently, with the B97-3c composite DFT method.<sup>14</sup> Geometries below 2 kcal/mol were then reoptimized with the PBEh-3c method. We pursued this strategy, since the B97-3c calculations could be performed faster than with the hybrid functional PBEh-3c. We verified these complex geometries as minima by reoptimization and Hessian calculations at the GFN2-xTB level. Starting from the  $S_0$  complex geometries obtained this way, the  $S_1$  exciplex geometries were optimized at the TDA-TDDFT/PBEh-3c level using the implementation available in Turbomole.<sup>15</sup> Only the lowest-lying conformer was considered for the calculation of vertical excitation and emission energies (see Figure S7). All structures are made available digitally in the archive that is uploaded with the supporting information this publication.

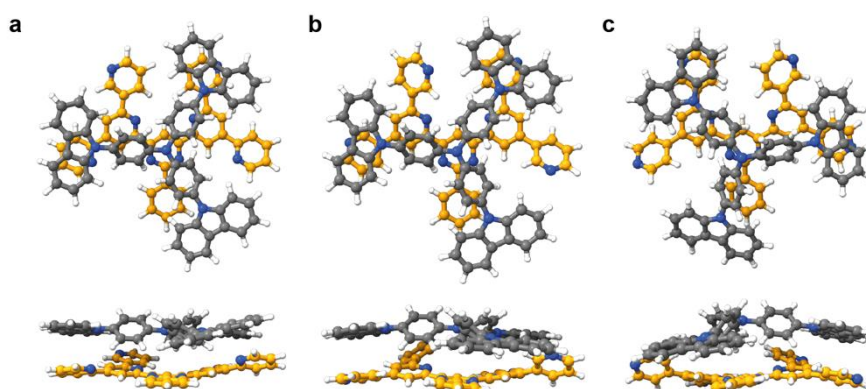


**Figure S7** | DFT-optimized structures of the TCTA:3,2'-BTP (a), TCTA:3,3'-BTP (b), and TCTA:3,4'-BTP (c) exciplexes as top and side views, with the BTP in orange and TCTA in grey. The shown geometries correspond to minima at the  $S_0$  potential energy surface.

## Simulation of the STM image of TCTA:3,4'-BTP

We first constructed a graphene sheet model with 256 carbon atoms, which was saturated with hydrogens at the edges (44 in total). After reoptimizing this geometry at the GFN2-xTB level, we docked the lowest-energy conformer of TCTA:3,4'-BTP onto the graphene sheet using the xTB-IFF force field. The lowest-energy structure determined from this docking procedure was then first reoptimized at the GFN2-xTB level, while constraining the bonds between the atoms marked in Figure S8. We constrained all distances connecting the capping hydrogens of the graphene sheet model during this optimization (using a harmonic potential with a force constant of 0.01 a.u.) to retain a mostly flat graphene surface, while not constraining the graphene carbon atoms themselves. After that, we performed a constrained molecular

dynamics (MD) simulation employing the force field method GFN-FF as implemented in the xTB code.<sup>16</sup> In addition to constraining the distances between the capping hydrogen atoms of the graphene model as before, we also constrained the distances between the atoms of the core pyrimidine unit of **3,4'-BTP** with the carbon atoms at the corners of the graphene sheet model (see Figure S8). The constraining was done to prevent large movements of the complex parallel to our comparably small graphene surface. We first equilibrated for 10 ps using an NVT ensemble (for  $T=298.15$  K) using the Berendsen thermostat.<sup>17</sup>

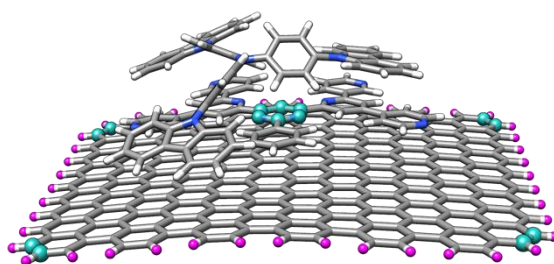


**Figure S8** | Starting geometry for the constrained MD simulation of TCTA:**3,4'-BTP** on a graphene sheet model. While the cyan atoms were kept fixed during the GFN-FF MD simulation, the capping hydrogen atoms (drawn in magenta) were also constrained during the preceding GFN2-xTB geometry optimization. This was achieved by constraining all distances between the (magenta) capping hydrogens, while for the cyan atoms, constraining was achieved by constraining the distances between the corner carbon atoms of the graphene sheet model and the pyrimidine unit atoms of **3,4'-BTP**.

After that, we performed a production run for 100 ps using an NVT ensemble (for  $T = 298.15$  K). We also applied an ellipsoid wall potential in which no force is applied to atoms that are within  $x \in [-40,40], y \in [-40,40], z \in [-30,30]$  (all distances in Bohr). A timestep of 2 fs was used throughout. To prevent too strong hydrogen movements due to this timestep, we increased the hydrogen mass by a factor of 4 by using the “hmass” keyword in the xTB code. From this constrained MD simulation, we extracted 100 equidistant structures and first aligned them along their respective principle moments of inertia as defined by all atoms of the graphene sheet and the constrained atoms of the **3,4'-BTP** pyrimidine unit. The resulting overlay of aligned structures is visualized in Figure S9.

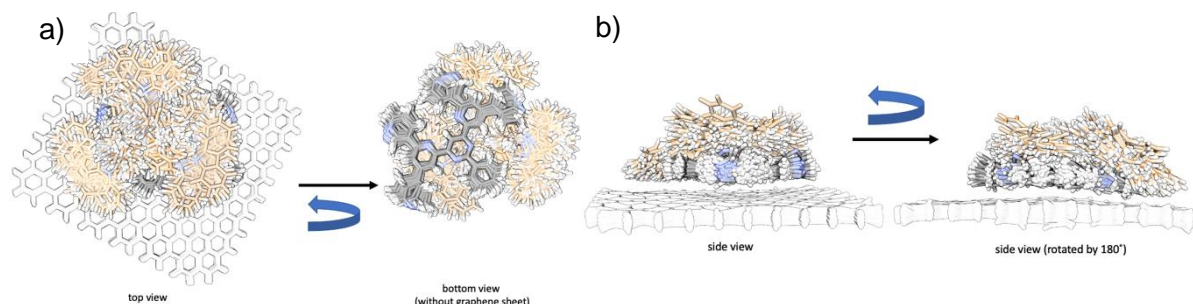


**Figure S9** | Overlay of sampled structures of TCTA:**3,4'-BTP** on a graphene sheet model. The structures are obtained from a constrained molecular dynamics (MD) simulation based on the GFN-FF force field (see text for details). In total, 100 equidistantly positioned carbon atoms were selected and used for the simulation of the STM image. Carbon atoms of **3,4'-BTP** are shown in dark gray and those of TCTA in orange. Views from a) the top and bottom and b) the side are shown.

We then computed an STM image for each of these structures using the GFN2-xTB method. The existing implementation in the xTB code based on the theory presented by Tersoff and Hamann is used for this purpose.<sup>18</sup> We then obtained the averaged STM image by convoluting the individual relative STM intensities obtained on a grid for each geometry with Gaussians of full width at half maximum of 0.1 Å. The alignment of structures as depicted in the top view (Figure S5a) was used to generate the STM images and all snapshot structures are made available digitally with this publication.

## STM investigation

### 3,4'-BTP

STM investigations of plain **3,4'-BTP** at the HOPG|TCB solution interface display well resolved lamellar patterns. As can be seen from Figure S4, many domains with various orientations at the HOPG|TCB solution interface are formed indicative of a strong interaction with the substrate leading to a high number of nuclei. The detailed view of Figure S10c suggests that at least five different morphologies exist. From the similarity of the short dimension of the unit cells of 1.9 to 2.0 nm it is assumed that four of those possess quite similar structures or are even identical. The rather different long dimensions between 3.1 and 3.4 nm, angles between 75° and 95° and contrast of those four patterns might be generated by drift effects and different orientations of the domains with respect to the scanning direction. The fifth morphology displays a unit cell of  $a = 3.7$  nm,  $b = 2.5$  nm,  $\alpha = 98^\circ$  which is significantly different from the previous values and is, thus, assigned to at least a second 2D structure.

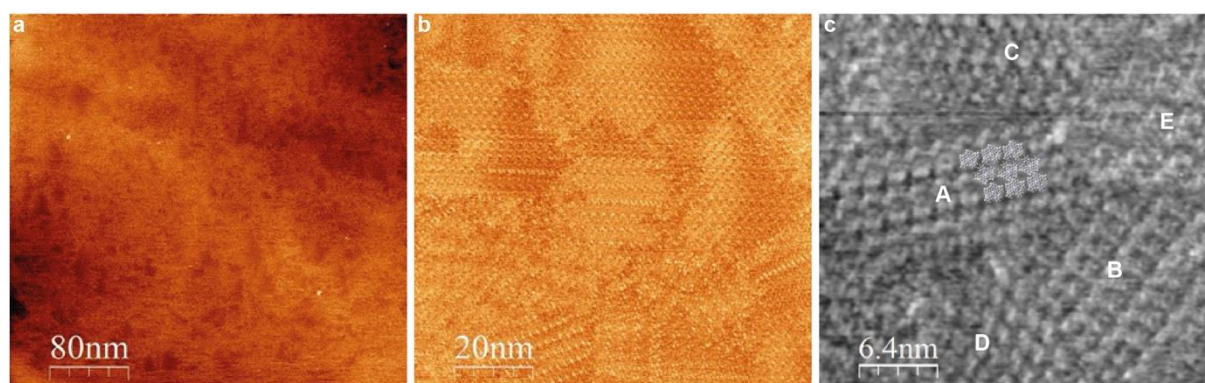


**Figure S10** | a,b) Overview images of **3,4'-BTP** at the HOPG|TCB solution interface displaying multidomain structures ( $U_T = -621$  mV (a) and  $U_T = -370$  mV (b)). c) Detailed view with assignment of different morphologies ( $U_T = -684$  mV; A:  $a = 3.2$  nm,  $b = 2.0$  nm,  $\alpha = 80^\circ$ ; B:  $a = 3.4$  nm,  $b = 1.9$  nm,  $\alpha = 75^\circ$ ; C:  $a = 3.1$  nm,  $b = 2.0$  nm,  $\alpha = 95^\circ$ ; D:  $a = 3.3$  nm,  $b = 1.9$  nm,  $\alpha = 90^\circ$ ; E:  $a = 3.7$  nm,  $b = 2.5$  nm,  $\alpha = 98^\circ$ ). It is assumed that A – D constitute the same morphology while E displays a different one.

Submolecular resolution from a further experiment (Figure S11a,b) allows an unambiguous assignment of a structure model 1 (Figure S11c,d) with a rectangular unit cell  $a = 3.4$  nm,  $b = 1.8$  nm,  $\alpha = 90^\circ$  bearing two molecules. We assume that the patterns A – D in Figure S10c correspond to this structure. From the intermolecular distances within one lamella we suggest weak C-H $\cdots$ N hydrogen bonds (Figure S11d) as known from self-assembled structures of the BTPs.<sup>19,20</sup> Unfortunately, despite the high resolution of the images no model could be assigned to the second structure E in Figure S11c.

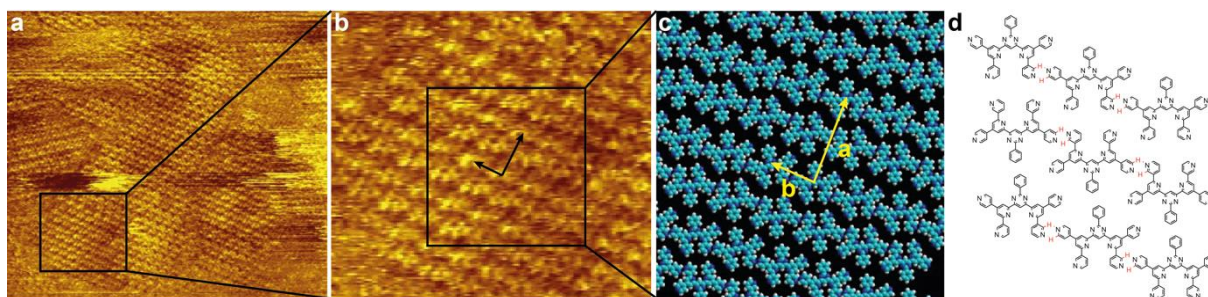


**Figure S11** | Plain **3,4'-BTP** at the HOPG|TCB solution interface with submolecular resolution and morphology 1. a) overview (80 x 80 nm<sup>2</sup>). b) Magnified view of a) ( $a = 3.4$  nm,  $b = 1.8$  nm,  $\alpha = 90^\circ$ ). c) Packing model with unit cell ( $a = 3.4$  nm,  $b = 1.8$  nm,  $\alpha = 90^\circ$ ). d) Tentative structure model 1 with intermolecular H bonds in red.

### TCTA:3,4'-BTP

At first TCTA alone was investigated but no regular structures could be detected by STM at the HOPG|TCB solution interface. Therefore, in the next step a TCTA solution in TCB was added to the already prepared HOPG|**3,4'-BTP** solution system. As in the case of plain **3,4'-BTP** (Figures S10, S11) multi-domain structures are found (Figure S12). Patches of dark areas are statistically distributed over the whole image in Figure S11a and surrounded by a medium bright background which bears regularly arranged bright spots. Detailed views in Figure S11b-d reveal that the dark areas are made up of highly regular patterns which consist of a dark structured background and bright structured spots. In contrast, the areas between the dark patches are also well-structured but are covered with more bright spots giving rise to the overall brighter appearance. Interestingly, the unit cell parameters of the various domains are in the same order as for the plain **3,4'-BTP** (Figure S10) with the short dimension between 1.8 and 2.0 nm and around 2.5 nm while the long one displays values between 3.2 and 3.9 nm. Thus, we assume that there is a monolayer of **3,4'-BTP** which is covered by a second layer either of **3,4'-BTP** or TCTA. A closer look on one domain shows that the bright spots of the second layer are not densely packed but the dimensions of the spots are in the expected range of single molecules (ca. 1.7 to 2.0 nm) for both **3,4'-BTP** and TCTA. Furthermore, the dark area is not fully covered and lines of the bright spots are “missing”. Those strong contrasts and specific patterns are not found for plain **3,4'-BTP**. Since the observed patterns furthermore match the STM image simulated by the force-field (GFN-FF) molecular dynamics simulations, we attribute them to the formation of TCTA:**3,4'-BTP** exciplexes (see main manuscript).

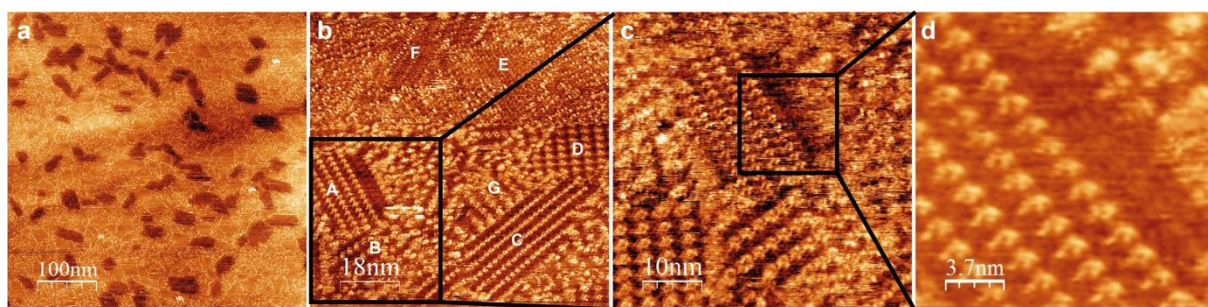


**Figure S12** | a) Overview image of the HOPG|**3,4'-BTP**,TcTa TCB solution interface. b) Detailed view with various domains (UT = -850 mV) A:  $a = 3.4$  nm,  $b = 1.8$  nm,  $\alpha = 75^\circ$ ; B:  $a = 3.5$  nm,  $b = 2.6$  nm,  $\alpha = 90^\circ$ ; C:  $a = 3.3$  nm,  $b = 2.0$  nm,  $\alpha = 75^\circ$ ; D:  $a = 3.9$  nm,  $b = 2.3$  nm,  $\alpha = 90^\circ$ ; E:  $a = 3.2$  nm,  $b = 2.5$  nm,  $\alpha = 90^\circ$ ; F:  $a = 3.2$  nm,  $b = 1.8$  nm,  $\alpha = 85^\circ$ ; G:  $a = 3.7$  nm,  $b = 2.30$  nm,  $\alpha = 85^\circ$ ). c,d) Detailed views of b) (UT = -850 mV; A:  $a = 3.4$  nm,  $b = 1.8$  nm,  $\alpha = 75^\circ$ ; B:  $a = 3.7$  nm,  $b = 2.5$  nm,  $\alpha = 90^\circ$ ; C:  $a = 3.7$  nm,  $b = 2.4$  nm,  $\alpha = 90^\circ$ ).

## Electroluminescence of TCTA:BTP exciplexes

### Experimental methods

#### *Mass spectrometry*

Matrix-assisted laser desorption/ionization (MALDI) high-resolution mass spectrometry (MS) was carried out on a Bruker solariX spectrometer using *trans*-2-[3-(4-tert-butylphenyl)-2-methyl-2-propenylidene]malononitrile (DCTB) as a matrix.

#### *Nuclear magnetic resonance spectroscopy*

NMR spectra were recorded on a 400 MHz and a 500 MHz NMR spectrometer from Bruker Corp.. The solvent signal was used as a reference with  $\delta(\text{CDCl}_3) = 7.26$  ppm and  $\delta(\text{DMSO-}d_6) = 2.50$  ppm.

#### *Photoluminescence spectroscopy*

Photoluminescence (PL) spectra and quantum yields of TCTA:**3,3'-BTP** exciplexes with different TCTA:BTP ratio were recorded on a PerkinElmer FL 6500 fluorescence photospectrometer.  $\Phi$  was determined using an integrating sphere at an excitation wavelength of 343 nm.

TCTA:3,N'-BTP films with thicknesses between 41 and 51 nm were thermally evaporated on 1 mm glass substrates. The substrates were cleaned 15 min in acetone and 15 min in isopropanol in the ultrasound bath. All films were encapsulated in a nitrogen-filled glovebox immediately after evaporation.

Angle-resolved photoluminescence spectra of each sample were acquired using a setup as described in literature.<sup>21</sup> The samples were coupled to a cylindrical glass lens using immersion oil and excited with a high-power LED with peak emission at 365 nm. The long-wavelength tail of the LED was cut using a short-pass filter with cut-off wavelength at 425 nm and spectra were acquired from 0° to 90°. The transverse electric (TE) component of the emission was blocked by a polarizer. The measured spectral radiant intensity emitted by these films was fitted to the following equation<sup>22</sup>

$$I(\theta, \lambda, a) = a \cdot I_{\text{TMv}} + \frac{1 - a}{2} \cdot I_{\text{TMh}}$$

where  $a$  is the free fitting parameter called anisotropy factor and  $I_{\text{TMv}}$  and  $I_{\text{TMh}}$  are the vertical and horizontal transverse magnetic components of the spectral radiant intensity, respectively. The latter quantities were calculated from a transfer-matrix method combined with an electromagnetic dipole model, as reported in the literature.<sup>23</sup>

Time-resolved photoluminescence spectra of the encapsulated TCTA:3,N'BTP films were measured with a time-correlated single photon counting (TCSPC) setup (FluoTime 250, TimeHarp 260, PMA Hybrid detector, PicoQuant) at room temperature with excitation wavelength at 373 nm. The detection was wavelength dependent ranging from 450 to 650 nm with a 5 nm resolution. The recorded time scales were 100  $\mu\text{s}$  with 51 ns resolution or 700 ns with 25 ps resolution.

#### *Scanning tunneling microscopy*

STM experiments were performed at ambient conditions with a commercially available low-current RHK SPM1000 STM with a resolution of 1024 x 1024 data points per image and scan speeds between 0.2 and 2  $\mu\text{m}\cdot\text{s}^{-1}$ . Generally, after cleaving the highly ordered pyrolytic graphite (HOPG) surface with adhesive tape, the quality of the mechanically cut Pt|Ir(80|20)

tip was tested through atomic resolution of the graphite surface. After stopping the scanning process, a drop (ca. 10  $\mu\text{L}$ ) of a saturated solution of the BTP or TCTA in TCB, respectively, was applied to the surface with the tip in tunnel contact. The applied tunneling current set point and bias voltage are specified in the figure captions. The STM images were subjected to slope subtraction, smoothing, and color correction (contrast, brightness). The data was evaluated with WSxM software.<sup>24</sup>

#### *OLED fabrication and characterization*

Display grade glass substrates with prepatterned ITO structure (90nm on Eagle XG glass, THIN FILM DEVICES) were cleaned with acetone and isopropyl alcohol in an ultrasonic bath and treated with oxygen plasma for 3 min. OLEDs were deposited in a high-vacuum thermal evaporator chamber (EvoVac, Angstrom Engineering Inc.) with a base pressure of  $10^{-7}$  mbar. Custom made shadow masks (LiMaB GmbH) for the organic and cathode layers produced pixels with an active area of  $4 \times 4 \text{ mm}^2$ . The device structure used in this study was as follows: ITO (90 nm) / 1,1-Bis[(di-4-tolylamino)phenyl]cyclohexane (TAPC, 60 nm)/ tris(4-carbazoyl-9-ylphenyl)amine (TCTA, 10 nm)/ TCTA:BTP (10:1, 30 nm)/ BTP (30 nm)/ LiF (1 nm)/ Al (100 nm). The devices were encapsulated like the thin films for characterization. The  $jV_L$  characteristics were measured by a source measurement unit (2400 SourceMeter, Keithley Instruments) and a calibrated silicon photodiode (PDA100A2, Thorlabs) connected to a sourcemeter (Keithley 2100). The electroluminescence spectra were recorded by a fiber-coupled OceanOptics Maya LSL. The evaluation of the data was performed taking into account Lambertian emission due to the bottom-emitting, ITO-based devices.

## **Materials**

TCTA was purchased from Luminescence Technology Corp. BTPs were synthesized similarly to previously described methods, starting from commercially (abcr GmbH and SigmaAldrich/Merck KGaA) available compounds and tributyl(1-ethoxyvinyl)stannane (synthesized as described by Soderquist *et al.*)<sup>19,25–29</sup> Commercially obtained chemicals were used without further purification. ITO coated substrates were prepared by Thin Film Devices Inc.

## **Synthetic procedures**

### 4,6-Dichloro-2-phenylpyrimidine (**2**)

Under argon atmosphere, 2-amino-4,6-dichloropyrimidine (**1**, 20.0 g, 122 mmol, 1.00 eq) and copper(I) oxide (17.5 g, 122 mmol, 1.00 eq) are suspended in anhydrous and degassed benzene (1 L). Isoamyl nitrite (60.6 mL, 451 mmol, 3.70 eq) is added to this suspension and the reaction mixture is subsequently heated to 70 °C and stirred for 4.5 h. After filtration of the reaction mixture and evaporation of the solvent under reduced pressure, the green crude product is purified by column chromatography ( $\text{SiO}_2$ , *n*-hexane/DCM 9:1  $\rightarrow$  8:2) to yield **2** (4.70 g, 20.9 mmol, 17%) as colorless solid.  $^1\text{H-NMR}$  (400 MHz,  $\text{CDCl}_3$ ):  $\delta$  [ppm] = 8.44 (dd,  $^3J_{\text{H,H}} = 8.3$ ,  $^4J_{\text{H,H}} = 1.4$  Hz, 2H), 7.62 – 7.42 (m, 3H), 7.28 (s, 1H).

### 1,1'-(2-Phenylpyrimidine-4,6-diyl)bis(ethan-1-one) (**3**)

Under argon atmosphere, a solution of **2** (4.70 g, 20.9 mmol, 1.00 eq), tributyl(1-ethoxyvinyl)stannane (17.4 g, 48.0 mmol, 2.30 eq), triphenylphosphine ( $\text{PPh}_3$ , 986 mg,

3.76 mmol, 0.18 eq), and tris(dibenzylideneacetone)dipalladium(0) ( $\text{Pd}_2(\text{dba})_3$ , 956 mg, 1.04 mmol, 0.05 eq) in degassed and anhydrous DMF (95 mL) is heated to 80 °C and stirred for 22 h. After cooling to room temperature, aqueous KF solution (7.05 g KF in 140 mL  $\text{H}_2\text{O}$ ) and diethyl ether (140 mL) are added and the mixture is stirred for 15 minutes. The mixture is extracted with diethyl ether (3x 200 mL), and the combined organic phases are dried over sodium sulfate. After evaporation of the solvent under reduced pressure, the dark brown solid is dissolved in acetone (150 mL), and hydrochloric acid (2M, 20 mL) is added. The reaction mixture is stirred for 22 h at room temperature, and then extracted with DCM (4x 200 mL). The combined organic phases are dried over  $\text{Na}_2\text{SO}_4$ , and the solvent is removed under reduced pressure. The obtained solid is purified *via* column chromatography ( $\text{SiO}_2$ , *n*-hexane/DCM 95:5  $\rightarrow$  0:100) to give **3** (4.70 g, 19.6 mmol, 94%).  $^1\text{H-NMR}$  (400 MHz,  $\text{CDCl}_3$ ):  $\delta$  [ppm] = 8.65 – 8.55 (m, 2H), 8.30 (s, 1H), 7.57 (dd,  $^3J_{\text{H,H}} = 5.2$ ,  $^4J_{\text{H,H}} = 1.8$  Hz, 3H), 2.85 (s, 6H).

#### 1,1'-((2-Phenylpyrimidine-4,6-diyl)bis(2-oxoethane-2,1-diyl))bis(pyridin-1-ium) diiodide (**4**)

A solution of iodine (3.15 g, 12.4 mmol, 1.99 eq) in anhydrous pyridine (7.5 mL) is added to a solution of **3** (1.50 g, 6.24 mmol, 1.00 eq) in anhydrous pyridine (7.5 mL). The reaction mixture is stirred at 100 °C for 4 h, cooled down to room temperature and stirred for 16 h at room temperature. The precipitate is filtered off and washed with cold DCM to yield the pyridinium salt **4** (2.48 g, 3.81 mmol, 61%) as ochre solid.  $^1\text{H-NMR}$  (400 MHz,  $\text{DMSO}-d_6$ ):  $\delta$  [ppm] = 9.02 (d,  $^3J_{\text{H,H}} = 5.9$  Hz, 4H), 8.82-8.73 (m, 4H), 8.33 (dd,  $^3J_{\text{H,H}} = 7.6$  Hz, 6.7 Hz, 4H), 8.16 (s, 1H), 7.76-7.74 (m, 3H), 6.73 (s, 4H).

#### 3-(Pyridin-2-yl)-1-(pyridin-3-yl)prop-2-en-1-one (**7a**)

Diethylamine (3.1 mL) is added to a solution of 3-acetylpyridine (3.30 mL, 30 mmol, 1.00 eq) and 2-pyridinecarboxaldehyde (2.85 mL, 30 mmol, 1.00 eq) in pyridine (6 mL), and the reaction mixture is stirred for 42 h at room temperature. After evaporation of the solvent under reduced pressure, the remaining dark green oil is diluted with DCM (50 mL) and washed with water (3x 50 mL). The organic phase is concentrated under reduced pressure, and within several days crystals are formed. The crystals are filtered off and rinsed with water (20 mL) to give the product (**7a**, 2.49 g, 11.9 mmol, 40%) as green solid.  $^1\text{H-NMR}$  (400 MHz,  $\text{CDCl}_3$ ):  $\delta$  [ppm] = 9.31 (d,  $^4J_{\text{H,H}} = 1.2$  Hz, 1H), 8.81 (dd,  $^3J_{\text{H,H}} = 4.7$  Hz,  $^4J_{\text{H,H}} = 1.5$  Hz, 1H), 8.71 (d,  $^3J_{\text{H,H}} = 4.5$  Hz, 1H), 8.36 (dt,  $^3J_{\text{H,H}} = 8.2$  Hz,  $^3J_{\text{H,H}} = 1.7$  Hz, 1H), 8.09 (d,  $^3J_{\text{H,H}} = 15.2$  Hz, 1H), 7.82 (d,  $^3J_{\text{H,H}} = 15.2$  Hz, 1H), 7.76 (dd,  $^3J_{\text{H,H}} = 7.5$  Hz,  $^4J_{\text{H,H}} = 1.4$  Hz, 1H), 7.50 (d,  $^3J_{\text{H,H}} = 7.6$  Hz, 1H), 7.46 (dd,  $^3J_{\text{H,H}} = 8.2$  Hz,  $^3J_{\text{H,H}} = 5.2$  Hz, 1H), 7.33 (dd,  $^3J_{\text{H,H}} = 7.6$  Hz,  $^3J_{\text{H,H}} = 4.7$  Hz, 1H).

#### 1,3-Di(pyridin-3-yl)prop-2-en-1-one (**7b**)

Diethylamine (3.1 mL) is added to a solution of 3-acetylpyridine (3.30 mL, 30 mmol, 1.00 eq) and 3-pyridinecarboxaldehyde (2.82 mL, 30 mmol, 1.00 eq) in pyridine (6 mL), and the reaction mixture is stirred for 80 h at room temperature. The resulting precipitate is filtered off and rinsed with water (50 mL) to give the product (**7b**, 3.45 g, 16.4 mmol, 55%) as yellow solid.  $^1\text{H-NMR}$  (400 MHz,  $\text{CDCl}_3$ ):  $\delta$  [ppm] = 9.24 (d,  $^4J_{\text{H,H}} = 2.2$  Hz, 1H), 8.87 (d,  $^4J_{\text{H,H}} = 2.2$  Hz, 1H), 8.83 (dd,  $^3J_{\text{H,H}} = 5.0$  Hz,  $^4J_{\text{H,H}} = 1.8$  Hz, 1H), 8.66 (dd,  $^3J_{\text{H,H}} = 4.8$  Hz,  $^4J_{\text{H,H}} = 1.6$  Hz, 1H), 8.31 (dt,  $^3J_{\text{H,H}} = 8.0$  Hz,  $^4J_{\text{H,H}} = 2.0$  Hz, 1H), 7.98 (dt,  $^3J_{\text{H,H}} = 8.0$  Hz,  $^4J_{\text{H,H}} = 1.9$  Hz, 1H), 7.84 (d,  $^3J_{\text{H,H}} = 15.9$  Hz, 1H), 7.57 (d,  $^3J_{\text{H,H}} = 15.9$  Hz, 1H), 7.49 (dd,  $^3J_{\text{H,H}} = 7.9$  Hz,  $^3J_{\text{H,H}} = 4.6$  Hz, 1H), 7.40 (dd,  $^3J_{\text{H,H}} = 8.1$  Hz,  $^3J_{\text{H,H}} = 4.9$  Hz, 1H).

### 1-(Pyridin-3-yl)-3-(pyridin-4-yl)prop-2-en-1-one (**7c**)

Diethylamine (3.1 mL) is added to a solution of 3-acetylpyridine (3.30 mL, 30 mmol, 1.00 eq) and 4-pyridinecarboxaldehyde (2.83 mL, 30 mmol, 1.00 eq) in pyridine (6 mL), and the reaction mixture is stirred for 5 days at room temperature. The resulting precipitate is filtered off and rinsed with water (50 mL). After recrystallization from water the product (**7c**, 320 mg, 1.52 mmol, 5%) is obtained as colorless solid. <sup>1</sup>H-NMR (400 MHz, CDCl<sub>3</sub>): δ [ppm] = 9.23 (d, <sup>4</sup>J<sub>H,H</sub> = 2.3 Hz, 1H), 8.83 (dd, <sup>3</sup>J<sub>H,H</sub> = 4.8 Hz, <sup>4</sup>J<sub>H,H</sub> = 1.9 Hz, 1H), 8.71 (dd, <sup>3</sup>J<sub>H,H</sub> = 4.1 Hz, <sup>4</sup>J<sub>H,H</sub> = 1.5 Hz, 2H), 8.30 (dt, <sup>3</sup>J<sub>H,H</sub> = 8.0 Hz, <sup>4</sup>J<sub>H,H</sub> = 2.0 Hz, 1H), 7.76 (d, <sup>3</sup>J<sub>H,H</sub> = 15.8 Hz, 1H), 7.63 (d, <sup>3</sup>J<sub>H,H</sub> = 15.8 Hz, 1H), 7.50-7.46 (m, 3H).

### 6',6'''-(2-Phenylpyrimidine-4,6-diyl)di-2,4':2',3''-terpyridine (**3,2'-BTP**)

A solution of **4** (250 mg, 385 μmol, 1.00 eq), **7a** (162 mg, 769 μmol, 2.00 eq), and ammonium acetate (1.5 g, 19.5 mmol, 51.0 eq) in methanol (8 mL) is heated to reflux and stirred for 20 h. The precipitate is collected *via* filtration and washed with methanol (50 mL) to give **3,2'-BTP** (111 mg, 179 μmol, 47%) as an ochre solid. The compound is further purified by sublimation (300°C, 10<sup>-5</sup> mbar). <sup>1</sup>H NMR (400 MHz, C<sub>2</sub>D<sub>2</sub>Cl<sub>4</sub>) δ 9.75 (s, 1H), 9.57 (d, <sup>4</sup>J<sub>H,H</sub> = 1.9 Hz, 2H), 9.25 (d, <sup>4</sup>J<sub>H,H</sub> = 1.3 Hz, 2H), 8.88 (m, 2H), 8.83 (m, 2H), 8.78 (dd, <sup>3</sup>J<sub>H,H</sub> = 4.8, <sup>4</sup>J<sub>H,H</sub> = 1.6 Hz, 2H), 8.73 (ddd, <sup>3</sup>J<sub>H,H</sub> = 8.0, <sup>4</sup>J<sub>H,H</sub> = 1.9 Hz, 2H), 8.67 (d, <sup>4</sup>J<sub>H,H</sub> = 1.4 Hz, 2H), 8.12 (m, 2H), 7.98 (ddd, <sup>3</sup>J<sub>H,H</sub> = 7.7, <sup>4</sup>J<sub>H,H</sub> = 1.8 Hz, 2H), 7.72 – 7.63 (m, 3H), 7.60 (dd, <sup>3</sup>J<sub>H,H</sub> = 8.1, 4.8 Hz, 2H), 7.49 (ddd, <sup>3</sup>J<sub>H,H</sub> = 7.5, 4.8, <sup>4</sup>J<sub>H,H</sub> = 1.1 Hz, 2H). MALDI-MS (DCTB, pos.): [M] = C<sub>40</sub>H<sub>26</sub>N<sub>8</sub>, experimental m/z = 619.23499 (found [M+H<sup>+</sup>]), calculated m/z = 619.23532.

### 6',6'''-(2-Phenylpyrimidine-4,6-diyl)di-3,2':4',3''-terpyridine (**3,3'-BTP**)

A solution of **4** (250 mg, 385 μmol, 1.00 eq), **7b** (162 mg, 769 μmol, 2.00 eq), and ammonium acetate (1.5 g, 19.5 mmol, 51.0 eq) in methanol (8 mL) is heated to reflux and stirred for 20 h. The precipitate is collected *via* filtration and washed with methanol (50 mL) to give **3,3'-BTP** (61 mg, 98 μmol, 26%) as an ochre solid. The compound is further purified by sublimation (300°C, 10<sup>-5</sup> mbar). <sup>1</sup>H NMR (400 MHz, C<sub>2</sub>D<sub>2</sub>Cl<sub>4</sub>) δ 9.74 (s, 1H), 9.54 (d, <sup>4</sup>J<sub>H,H</sub> = 1.9 Hz, 2H), 9.15 (d, <sup>4</sup>J<sub>H,H</sub> = 1.8 Hz, 2H), 9.00 (d, *J* = 1.5 Hz, 2H), 8.86 – 8.75 (m, 6H), 8.67 (ddd, <sup>3</sup>J<sub>H,H</sub> = 8.1, <sup>4</sup>J<sub>H,H</sub> = 2.1 Hz, 2H), 8.25 – 8.17 (m, 2H), 8.15 (d, *J* = 1.6 Hz, 2H), 7.76 – 7.52 (m, 7H). MALDI-MS (DCTB, pos.): [M] = C<sub>40</sub>H<sub>26</sub>N<sub>8</sub>, experimental m/z = 619.23493 (found [M+H<sup>+</sup>]), calculated m/z = 619.23532.

### 6',6'''-(2-Phenylpyrimidine-4,6-diyl)di-3,2':4',4''-terpyridine (**3,4'-BTP**)

A solution of **4** (250 mg, 385 μmol, 1.00 eq), **7c** (162 mg, 769 μmol, 2.00 eq), and ammonium acetate (1.5 g, 19.5 mmol, 51.0 eq) in methanol (8 mL) is heated to reflux and stirred for 20 h. The precipitate is collected *via* filtration and washed with methanol (50 mL) to give **3,4'-BTP** (139 mg, 225 μmol, 58%) as colorless solid. The compound is further purified by sublimation (300°C, 10<sup>-5</sup> mbar). <sup>1</sup>H NMR (400 MHz, C<sub>2</sub>D<sub>2</sub>Cl<sub>4</sub>) δ 9.72 (s, 1H), 9.53 (d, <sup>4</sup>J<sub>H,H</sub> = 1.8 Hz, 2H), 9.00 (d, <sup>4</sup>J<sub>H,H</sub> = 1.5 Hz, 2H), 8.90 – 8.84 (m, 4H), 8.84 – 8.75 (m, 4H), 8.69 (ddd, <sup>3</sup>J<sub>H,H</sub> = 8.0, <sup>4</sup>J<sub>H,H</sub> = 1.9 Hz, 2H), 8.17 (d, <sup>4</sup>J<sub>H,H</sub> = 1.6 Hz, 2H), 7.85 – 7.78 (m, 4H), 7.71 – 7.57 (m, 5H). MALDI-MS (DCTB, pos.): [M] = C<sub>40</sub>H<sub>26</sub>N<sub>8</sub>, experimental m/z = 619.23489 (found [M+H<sup>+</sup>]), calculated m/z = 619.23532.

### NMR spectra

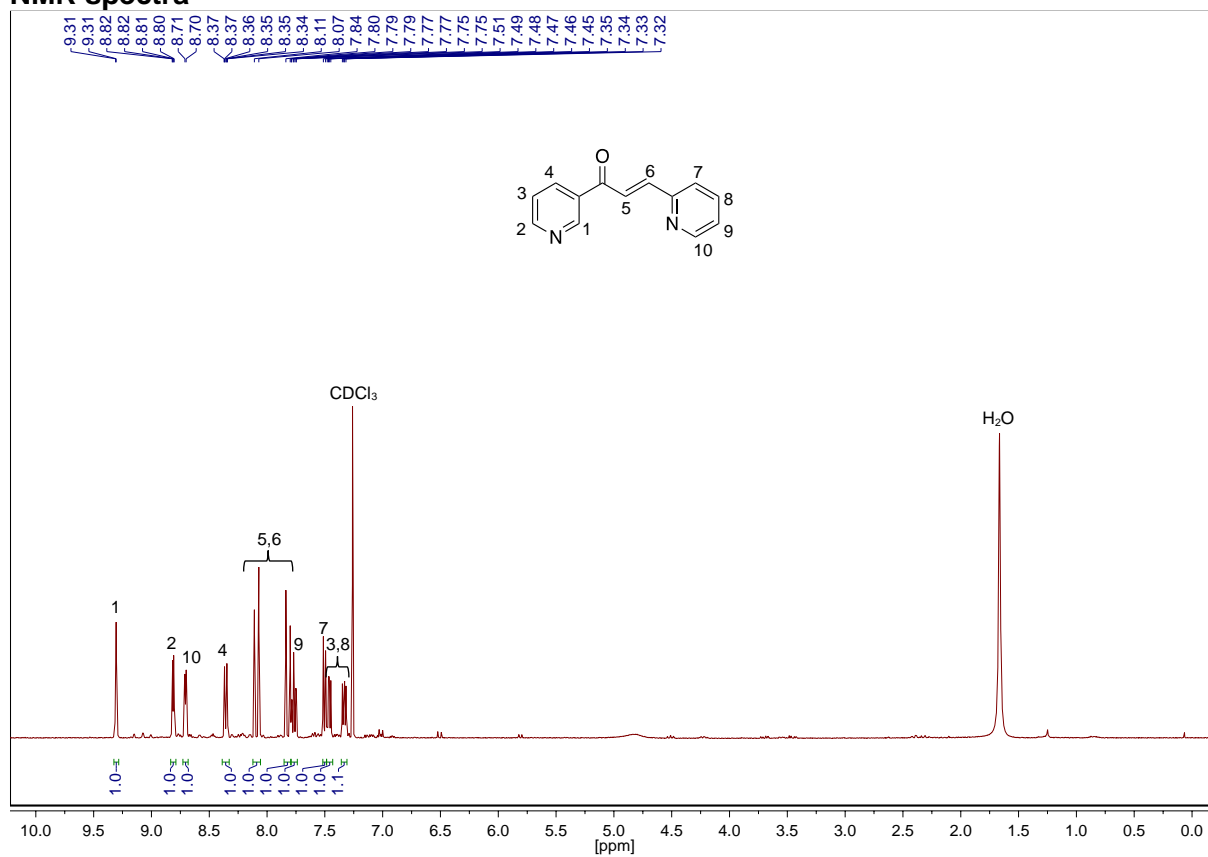


Figure 13 <sup>1</sup>H-NMR spectrum of compound 5a in CDCl<sub>3</sub>.

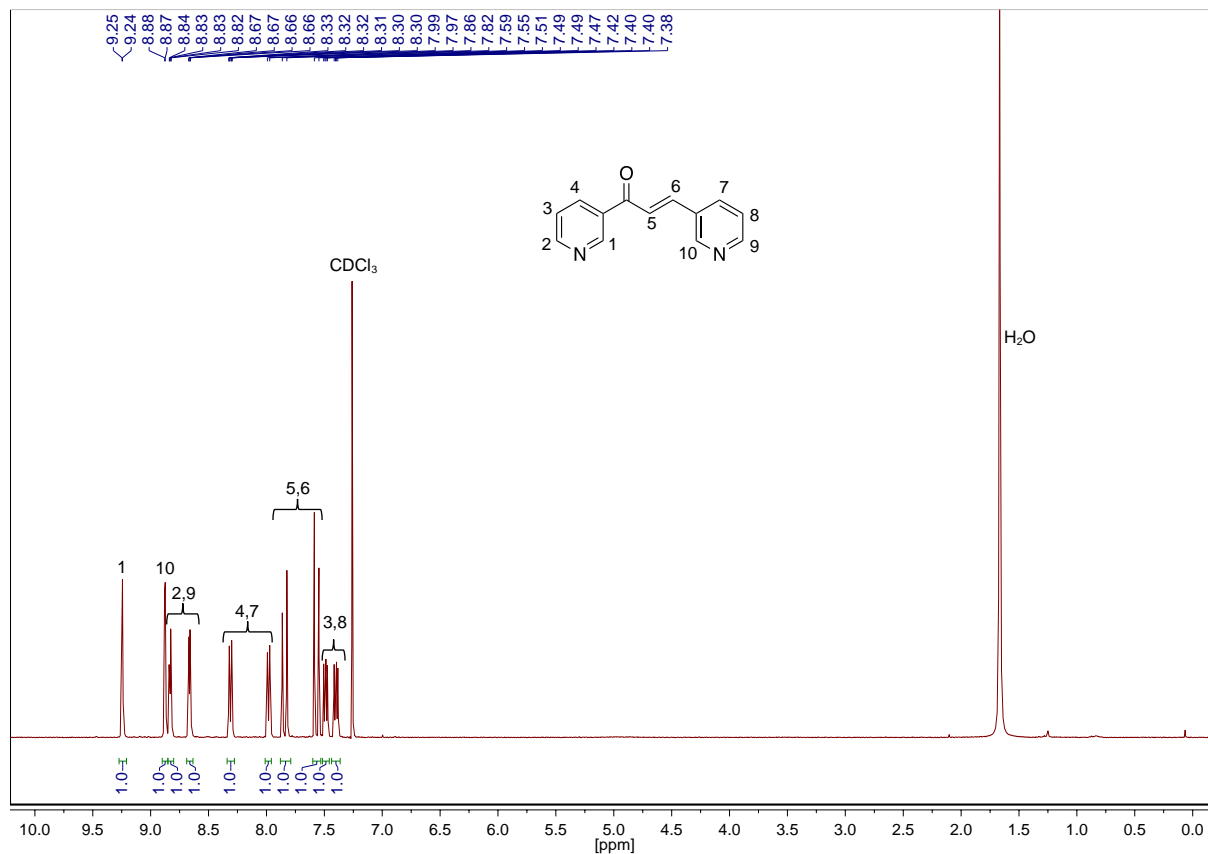


Figure S14 | <sup>1</sup>H-NMR spectrum of compound 5b in CDCl<sub>3</sub>.

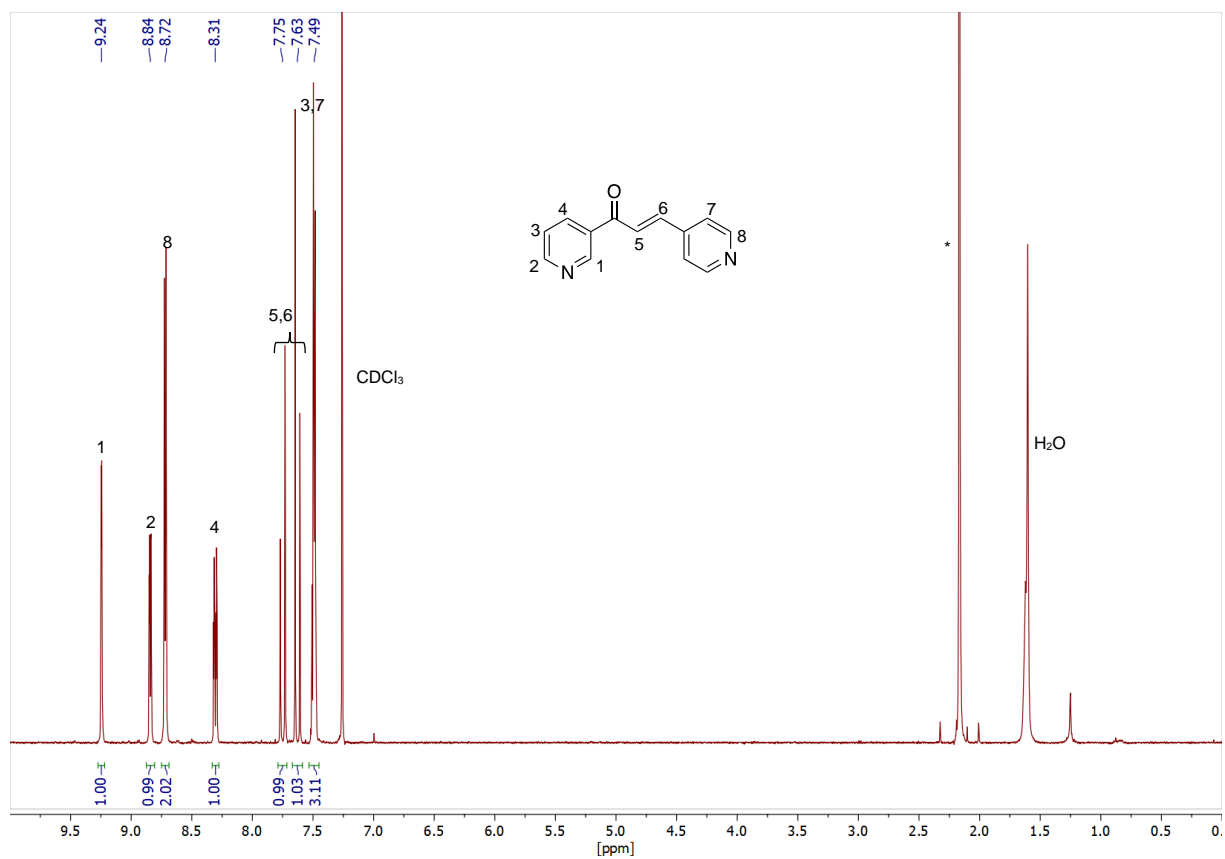


Figure S15 | <sup>1</sup>H-NMR spectrum of compound **5c** in CDCl<sub>3</sub>.

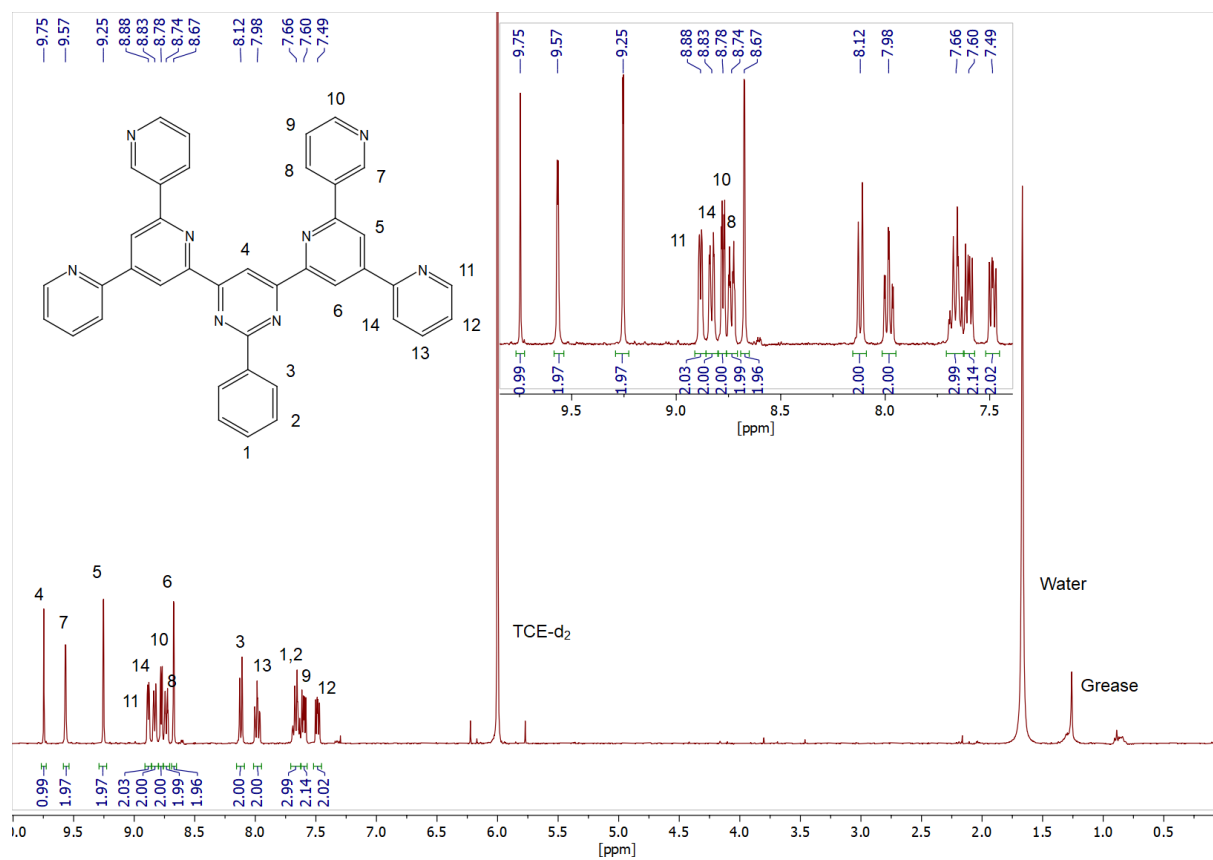


Figure S16 | <sup>1</sup>H-NMR spectrum of compound **3,2'-BTP** in TCE-d<sub>2</sub>.

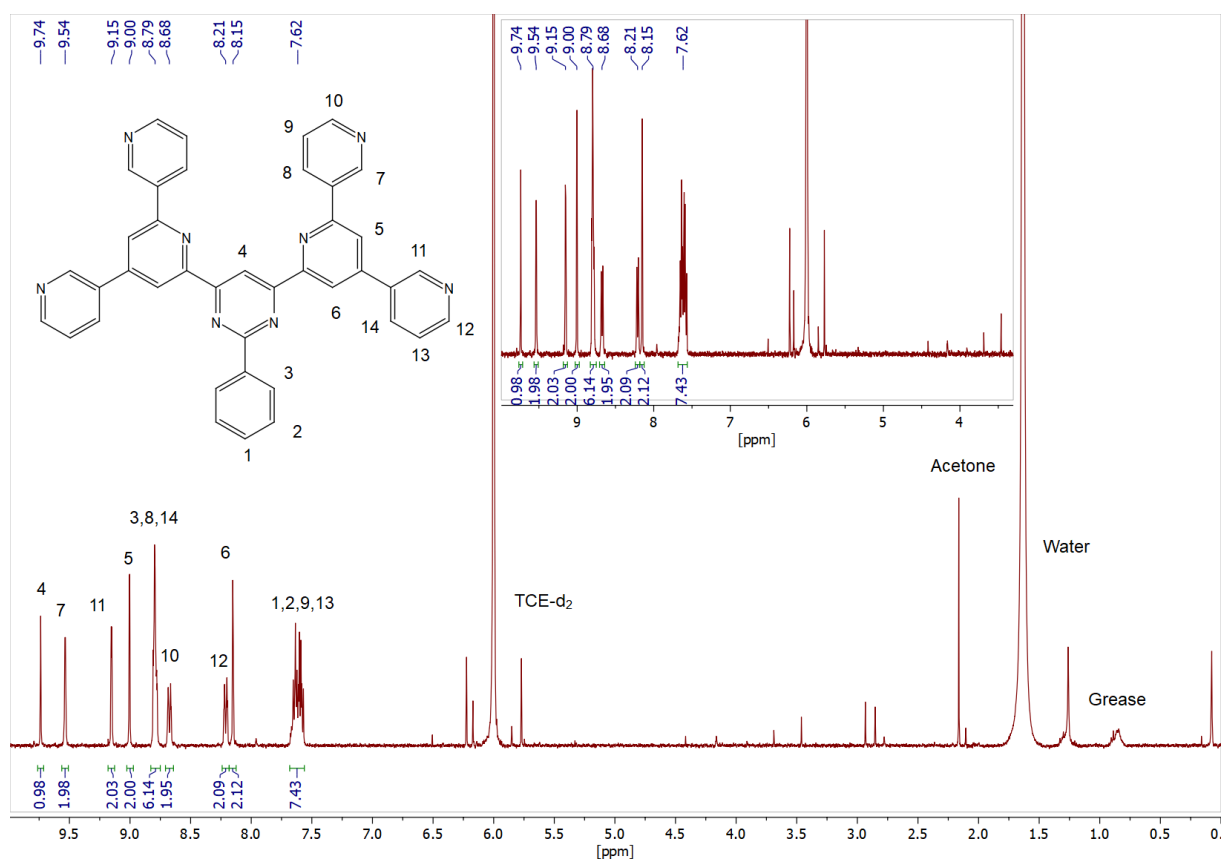


Figure S17 |  $^1\text{H-NMR}$  spectrum of compound 3,3'-BTP in  $\text{TCE-d}_2$ .

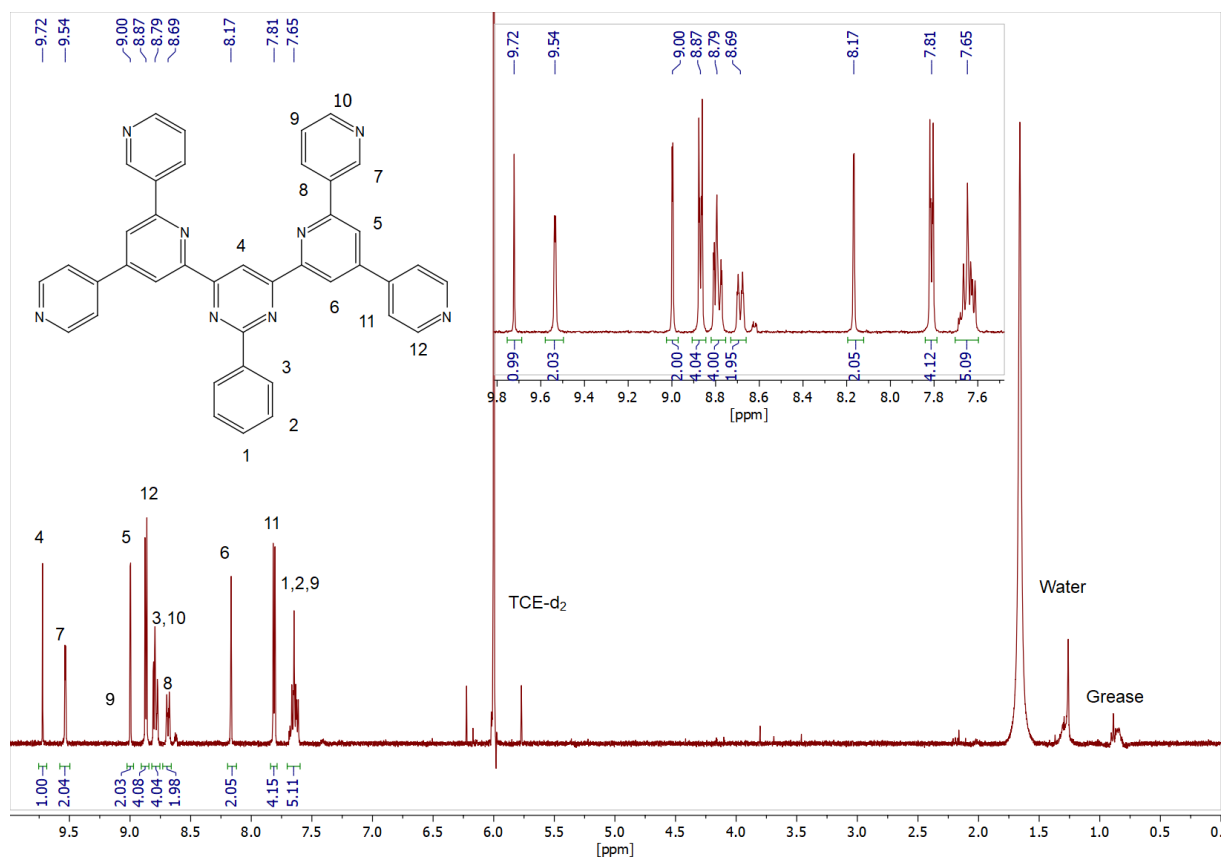
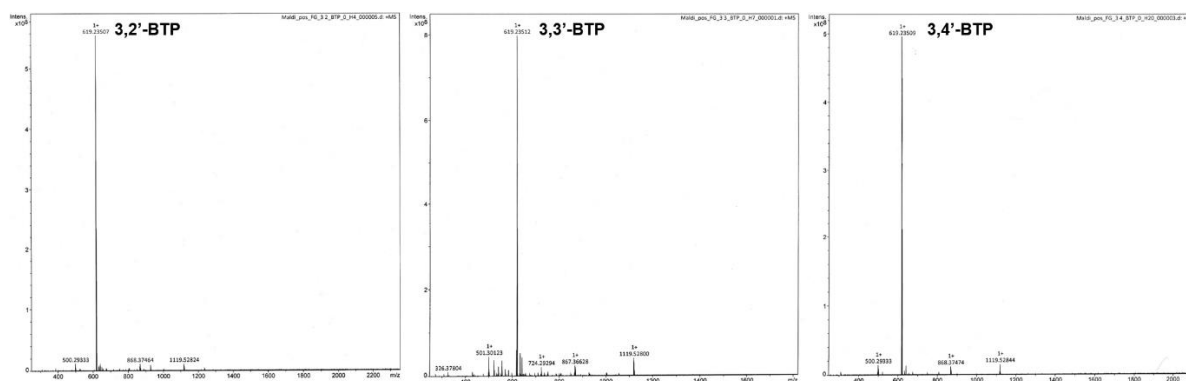


Figure S18 |  $^1\text{H-NMR}$  spectrum of compound 3,4'-BTP in  $\text{TCE-d}_2$ .



**Figure S19** | MALDI-ToF mass spectrometry results of the BTPs purified by sublimation.

### **Computational Study:**

#### **Calculation of vertical ionization and excitation energies of the BTP and TCTA monomers:**

Having computed the ground state minima of the individual BTP and TCTA molecules at the PBEh-3c (cf. simulation of the exciplexes),<sup>7</sup> we compute vertical ionization potentials and electron affinities according to

$$IP = E(A^+) - E(A)$$

and

$$EA = E(A) - E(A^-).$$

For a better description of both the ionic and neutral forms, we chose to use a larger basis set than included within the composite PBEh-3c method: we employ the PBE0/def2-TZVP level of theory<sup>30,31</sup> for the respective single-point calculations – restricted for the neutral states and unrestricted for the ionic states. The results are given in the table below.

Furthermore, vertical excitation energies are computed for the monomers at the Tamm-Dancoff-approximated DFT level<sup>32</sup> employing the PBEh-3c level of theory.

	$E(A)$ [ $E_h$ ]	$E(A^+)$ [ $E_h$ ]	$E(A^-)$ [ $E_h$ ]	$IP$ [eV]	$EA$ [eV]	gap [eV]	$E_{S_0 \rightarrow S_1}$ [eV] <sup>a)</sup>
3,2'-BTP	-1976.45414	-1976.17313	-1976.49936	7.6	1.2	6.5	4.3
3,3'-BTP	-1976.44719	-1976.15956	-1976.49617	7.8	1.3	6.5	4.3
3,4'-BTP	-1976.44720	-1976.15691	-1976.49964	7.9	1.4	6.5	4.3
TCTA	-2296.74976	-2296.51488	-2296.76117	6.4	0.3	6.1	4.2

<sup>a)</sup> Computed for the neutral system at the TDA-PBEh-3c//PBEh-3c level. All other values are computed vertically at the PBE0/def2-TZVP level on the PBEh-3c  $S_0$  geometry.

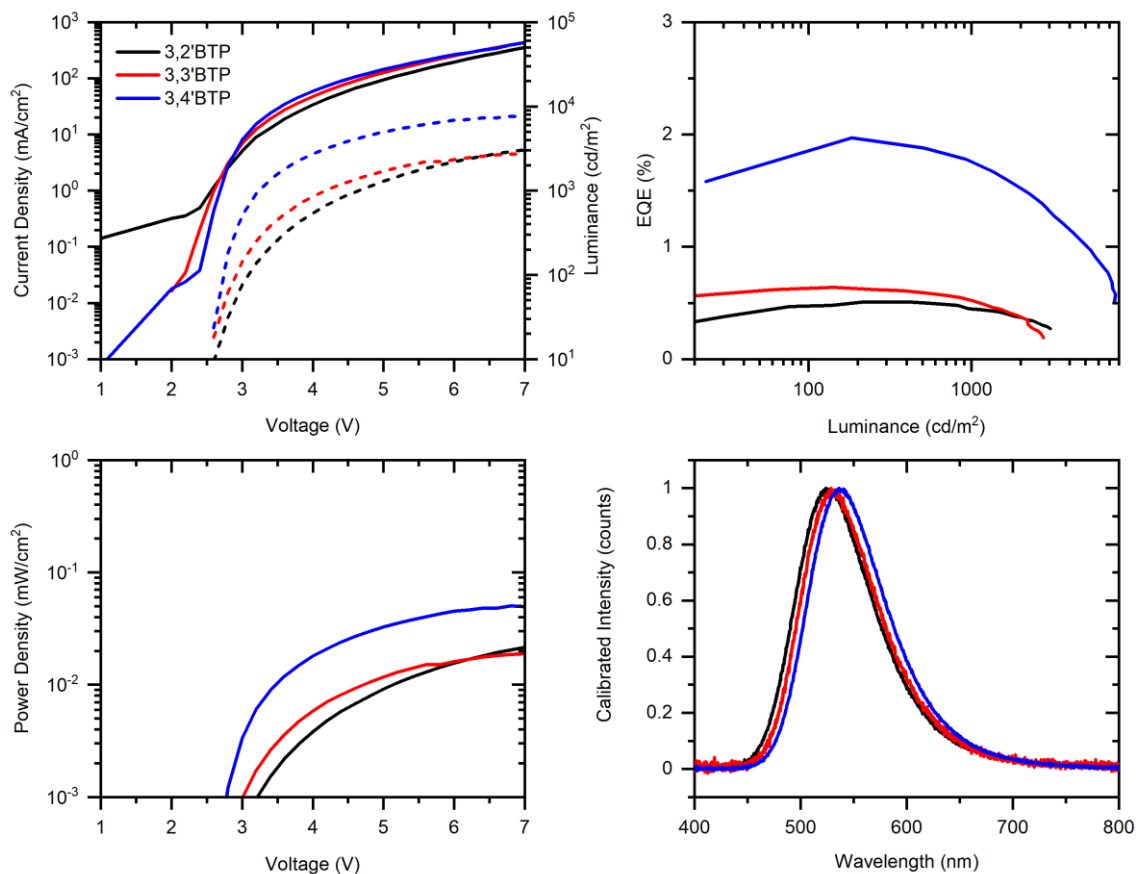


**Figure S20** | (a) Current density and luminance plotted against the applied voltage of the bottom-emitting OLEDs. (b) External quantum efficiency in % plotted against luminance. (c) Power density versus voltage. (d) Normalized electroluminescence spectra. All data color-coded with 3,2'BTP (black), 3,3'BTP (red) and 3,4'BTP (blue).



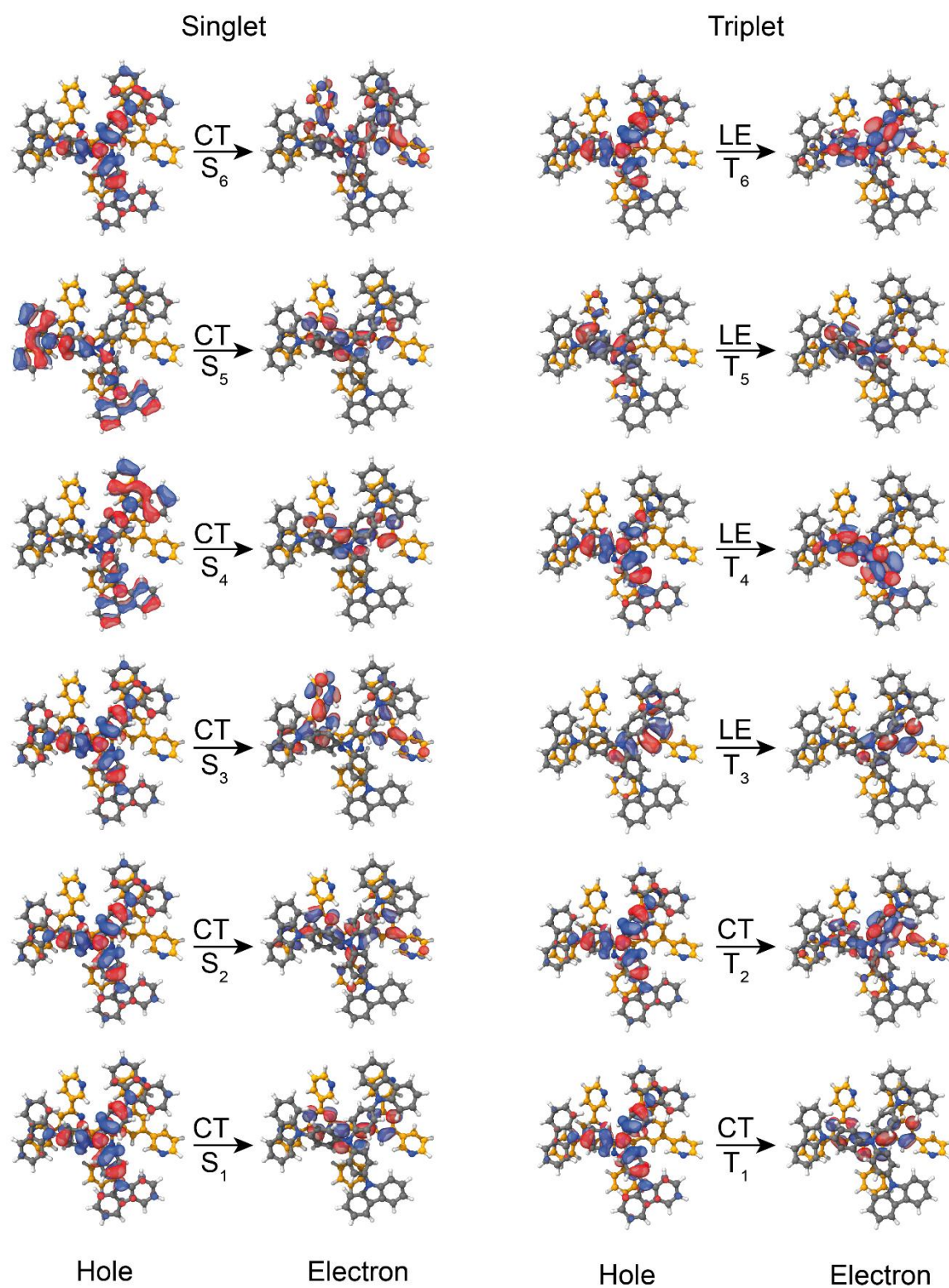


**Figure S22** | Visual representation of the NTOs of the TCTA:3,3'-BTP exciplex for its respective first singlet and triplet states.

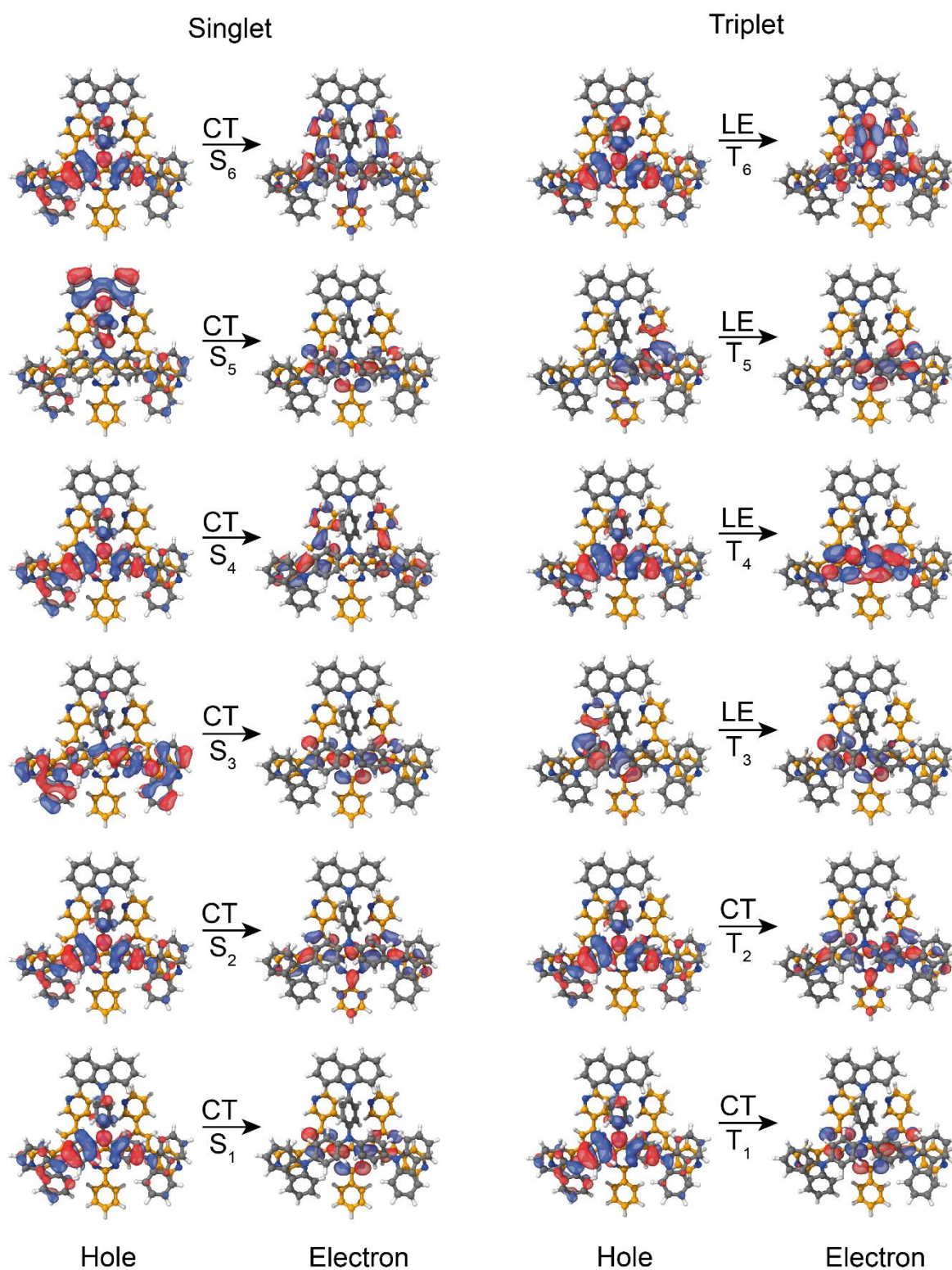


**Figure S23** | Visual representation of the NTOs of the TCTA:3,4'-BTP exciplex for its respective first singlet and triplet states.

Coordinates for the individual optimized molecular structures of compounds 3,2'-BTP, 3,3'-BTP, 3,4'-BTP, TCTA as well as for the exciplexes (TCTA:3,2'-BTP, TCTA:3,3'-BTP, TCTA:3,4'-BTP) are supplied in a separate supplementary zip-file.

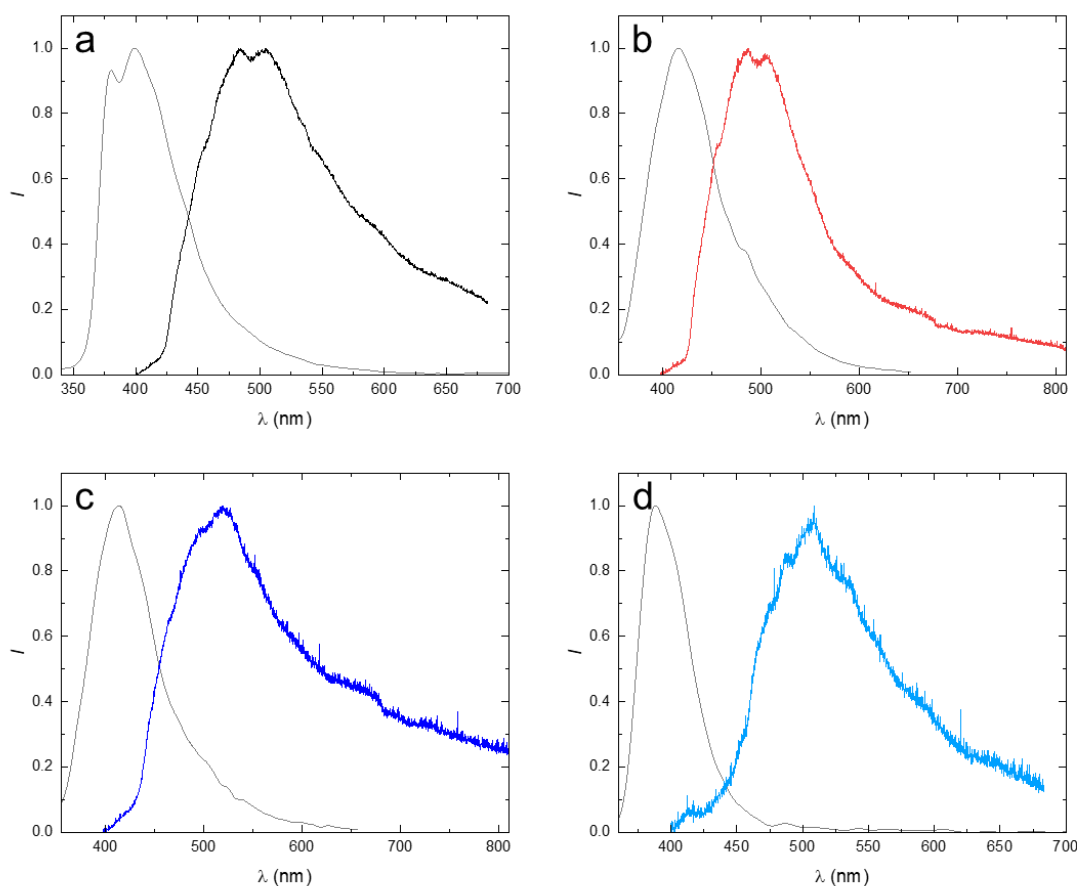


**Figure S24** | Fluorescence (grey) and phosphorescence spectra (color coded) of a) 3,2'-BTP, b) 3,3'-BTP, c) 3,4'-BTP and d) TCTA. All spectra recorded at 355 nm excitation in chloroform solution. Phosphorescence spectra recorded at -196 °C.

## References

- 1 J. L. Solomon, R. J. Madix and J. Stöhr, *Surf. Sci.*, 1991, **255**, 12–30.
- 2 A. C. Liu and C. M. Friend, *J. Chem. Phys.*, 1988, **89**, 4396–4405.
- 3 P. Pracht, F. Bohle and S. Grimme, *Phys. Chem. Chem. Phys.*, 2020, **22**, 7169–7192.
- 4 C. Bannwarth, S. Ehlert and S. Grimme, *J. Chem. Theory Comput.*, 2019, **15**, 1652–1671.
- 5 CREST code: <https://github.com/grimme-lab/crest> (last accessed: 27.09.2021).
- 6 xTB code: <https://github.com/grimme-lab/xtb> (last accessed: 27.09.2021).
- 7 S. Grimme, J. G. Brandenburg, C. Bannwarth and A. Hansen, *J. Chem. Phys.*, 2015, **143**, 054107.
- 8 S. Grimme, J. Antony, S. Ehrlich and H. Krieg, *J. Chem. Phys.*, 2010, **132**, 154104.

- 9 S. Grimme, S. Ehrlich and L. Goerigk, *J. Comput. Chem.*, 2011, **32**, 1456–1465.
- 10 H. Kruse and S. Grimme, *J. Chem. Phys.*, 2012, **136**, 154101.
- 11 F. Furche, R. Ahlrichs, C. Hättig, W. Klopper, M. Sierka and F. Weigend, *WIREs Comput. Mol. Sci.*, 2014, **4**, 91–100.
- 12 S. Grimme, C. Bannwarth, E. Caldeweyher, J. Pisarek and A. Hansen, *J. Chem. Phys.*, 2017, **147**, 161708.
- 13 S. Grimme, C. Bannwarth and P. Shushkov, *J. Chem. Theory Comput.*, 2017, **13**, 1989–2009.
- 14 J. G. Brandenburg, C. Bannwarth, A. Hansen and S. Grimme, *J. Chem. Phys.*, 2018, **148**, 064104.
- 15 S. Hirata and M. Head-Gordon, *Chem. Phys. Lett.*, 1999, **314**, 291–299.
- 16 S. Spicher and S. Grimme, *Angew. Chemie*, 2020, **132**, 15795–15803.
- 17 H. J. C. Berendsen, J. P. M. Postma, W. F. van Gunsteren, A. DiNola and J. R. Haak, *J. Chem. Phys.*, 1984, **81**, 3684–3690.
- 18 J. Tersoff and D. R. Hamann, *Phys. Rev. Lett.*, 1983, **50**, 1998–2001.
- 19 C. Meier, U. Ziener, K. Landfester and P. Wehrich, *J. Phys. Chem. B*, 2005, **109**, 21015–21027.
- 20 U. Ziener, *J. Phys. Chem. B*, 2008, **112**, 14698–14717.
- 21 E. Archer, S. Hillebrandt, C. Keum, C. Murawski, J. Murawski, F. Tenopala-Carmona and M. C. Gather, *Adv. Opt. Mater.*, 2021, **9**, 2000838.
- 22 P. Liehm, C. Murawski, M. Furno, B. Lüssem, K. Leo and M. C. Gather, *Appl. Phys. Lett.*, 2012, **101**, 253304.
- 23 M. Furno, R. Meerheim, S. Hofmann, B. Lüssem and K. Leo, *Phys. Rev. B*, 2012, **85**, 115205.
- 24 I. Horcas, R. Fernández, J. M. Gómez-Rodríguez, J. Colchero, J. Gómez-Herrero and A. M. Baro, *Rev. Sci. Instrum.*, 2007, **78**, 013705.
- 25 J. A. Soderquist and G. J. H. Hsu, *Organometallics*, 1982, **1**, 830–833.
- 26 U. Ziener, J.-M. Lehn, A. Mourran and M. Möller, *Chem. - A Eur. J.*, 2002, **8**, 951–957.
- 27 J. Durinda, L. Szücs, L. Krasnec, J. Heger, V. Springer, J. Kolena and J. Keleti, *Acta Fac. Pharm. Bohem.*, 1966, **12**, 89–129.
- 28 A. Attia and M. Michael, *Pharmazie*, 1982, **37**, 551–553.
- 29 B. Eggers and U. Ziener, *Chem. - A Eur. J.*, 2018, **24**, 14968–14973.
- 30 C. Adamo and V. Barone, *J. Chem. Phys.*, 1999, **110**, 6158–6170.
- 31 F. Weigend and R. Ahlrichs, *Phys. Chem. Chem. Phys.*, 2005, **7**, 3297–3305.
- 32 S. Hirata and M. Head-Gordon, *Chem. Phys. Lett.*, 1999, **314**, 291–299.